



HAL
open science

High-harmonic generation in solids from a high-energy fiber laser system

D. Boukhaoui, A. Mikhneva, S. Idlahcen, J. Houard, T. Godin, L. Guiramand, I. Blum, F. Amrani, F. Gérôme, F. Benabid, et al.

► **To cite this version:**

D. Boukhaoui, A. Mikhneva, S. Idlahcen, J. Houard, T. Godin, et al.. High-harmonic generation in solids from a high-energy fiber laser system. *APL Photonics*, 2025, 10 (2), pp.026106. 10.1063/5.0244415 . hal-04933912

HAL Id: hal-04933912

<https://hal.science/hal-04933912v1>

Submitted on 7 Feb 2025

HAL is a multi-disciplinary open access archive for the deposit and dissemination of scientific research documents, whether they are published or not. The documents may come from teaching and research institutions in France or abroad, or from public or private research centers.













L'archive ouverte pluridisciplinaire **HAL**, est destinée au dépôt et à la diffusion de documents scientifiques de niveau recherche, publiés ou non, émanant des établissements d'enseignement et de recherche français ou étrangers, des laboratoires publics ou privés.



Distributed under a Creative Commons Attribution 4.0 International License

RESEARCH ARTICLE | FEBRUARY 06 2025

High-harmonic generation in solids from a high-energy fiber laser system

D. Boukhaoui ; A. Mikhneva; S. Idlahcen ; J. Houard ; T. Godin  ; L. Guiramand ; I. Blum ; F. Amrani; F. Gérôme ; F. Benabid; D. Gauthier; W. Boutu ; H. Merdji ; A. Vella ; A. Hideur 



APL Photonics 10, 026106 (2025)

<https://doi.org/10.1063/5.0244415>



View
Online



Export
Citation

Articles You May Be Interested In

Generation of low power and ultrashort laser pulses at 800 nm through soliton compression in chloroform-infiltrated cascaded photonic crystal fibers

J. Appl. Phys. (September 2018)

Efficient spectral broadening of supercontinuum in photonic crystal fiber with self-phase modulation induced by femtosecond laser pulse

Appl. Phys. Lett. (November 2012)

Enhanced extreme ultraviolet high-harmonic generation from chromium-doped magnesium oxide

Appl. Phys. Lett. (May 2021)



APL Photonics

Special Topics Open
for Submissions

[Learn More](#)

High-harmonic generation in solids from a high-energy fiber laser system

Cite as: APL Photon. 10, 026106 (2025); doi: 10.1063/5.0244415

Submitted: 18 October 2024 • Accepted: 26 January 2025 •

Published Online: 6 February 2025

















View Online



Export Citation



CrossMark

D. Boukhaoui,¹  A. Mikhneva,^{1,2}  S. Idlahcen,²  J. Houard,¹  T. Godin,^{2,a)}  L. Guiramand,² 
I. Blum,¹  F. Amrani,³ F. Gérôme,^{3,4}  F. Benabid,^{3,4}  D. Gauthier,^{5,6}  W. Boutu,^{5,6}  H. Merdji,⁷ 
A. Vella,¹  and A. Hideur^{2,b)} 

AFFILIATIONS

¹GPM UMR 6634, CNRS - University of Rouen Normandie - INSA Rouen Normandie, Rouen, France

²CORIA UMR 6634, CNRS - University of Rouen Normandie - INSA Rouen Normandie, Rouen, France

³Glophotonics, 123 avenue Albert Thomas, 87060 Limoges Cedex, France

⁴GPPMM Group, XLIM Research Institute, CNRS UMR 7252, University of Limoges, Limoges, France

⁵Université Paris-Saclay, CEA, LIDYL, 91191 Gif sur Yvette, France

⁶CY Cergy Paris Université, CEA, LIDYL, 91191 Gif sur Yvette, France

⁷Laboratoire d'Optique Appliquée, CNRS, Ecole Polytechnique, ENSTA, Institut Polytechnique de Paris, Palaiseau, France

^{a)} Author to whom correspondence should be addressed: thomas.godin@coria.fr

^{b)} Electronic mail: hideur@coria.fr

ABSTRACT

We demonstrate high-harmonic generation (HHG) in solids using a high-energy fiber laser system operating at 1550 nm. The driving few-cycle source consists of an erbium-doped fiber chirped pulse amplifier combined with a post-compression stage featuring a gas-filled hollow-core photonic crystal fiber (HC-PCF). The nonlinear self-compression process in the HC-PCF enables the generation of ultrashort pulses with sub-50 fs durations and μJ -level energies at a 660 kHz repetition rate. Perturbative and non-perturbative harmonics were subsequently generated when focusing the few-cycle pulses into zinc oxide (ZnO) and magnesium oxide (MgO) bulk samples. In the latter, in particular, we observed the generation of extreme ultraviolet harmonics up to H29 (below 55 nm), highlighting the remarkable potential of such a platform for the development of compact HHG sources.

© 2025 Author(s). All article content, except where otherwise noted, is licensed under a Creative Commons Attribution-NonCommercial 4.0 International (CC BY-NC) license (<https://creativecommons.org/licenses/by-nc/4.0/>). <https://doi.org/10.1063/5.0244415>

I. INTRODUCTION

Over the past few decades, the development of high-energy ultrafast lasers delivering few-cycle light pulses has enabled several breakthroughs in spectroscopy and the tailoring of light-matter interactions. In particular, high-harmonic generation (HHG)¹ has enabled the development of coherent extreme ultraviolet (EUV) light sources through nonlinear conversion.^{2–5} HHG, resulting from the nonlinear interaction of an intense laser field with an atomic or molecular gas, has led to significant advances in ultrafast science, particularly in the generation of high-energy photons and isolated attosecond pulses,^{6–9} tomographic imaging of molecules,^{10–16} and high-resolution spectroscopy,^{17–21} to cite a few.

A major breakthrough occurred in 2011 with the demonstration of low-threshold HHG in a bulk zinc oxide (ZnO) crystal using few-cycle mid-IR pulses.²² The generation mechanism involves inter- and intra-band electron dynamics, resulting in bright vacuum ultraviolet (VUV) and EUV emissions.²³ Thus, HHG in solids represents an attractive route toward compact tabletop sources of coherent and bright attosecond pulses in the EUV energy range, which are key tools for probing the electron dynamics in crystalline and amorphous media.^{23–32}

HHG is strongly dependent on the driving wavelength. While in gases, the high harmonic cut-off (the highest frequency in the harmonic spectrum) depends on the square of the driving wavelength, in solids, it depends linearly on the field strength.^{32,33} The use of

long wavelength pulses extends the cut-off and increases the damage threshold of bulk crystals. Such conditions were achieved using high-power laser systems combined with optical parametric chirped pulse amplifiers (OPCPAs)^{22,34–36} and optical parametric amplifiers (OPAs).^{37–42} OPCPA architectures offer high energy levels in the few-cycle pulse regime, but they have complex configurations and generally operate at low repetition rates. The use of ultrafast fiber lasers in the mid-IR is a very promising way to develop ultra-compact HHG platforms. This has been confirmed by several demonstrations of HHG driven by few-cycle mid-IR fiber lasers.^{43–45} However, these sources based on soliton self-frequency shift or supercontinuum generation in all-solid fibers are limited to a few tens of nanojoules.

The best solution for achieving high energy levels in an all-fiber configuration involves the use of post-compression in hollow core (HC) photonic crystal fibers (PCFs) filled with noble gases.⁴⁷ Such fibers offer the best self-compression qualities due to their high non-linearity to ionization rate ratio and do not exhibit a delayed Raman response, as they use an atomic gas. Compared to traditional pulse compression methods based on solid-core optical fibers, hollow-core fibers support single mode operation with larger mode sizes and thus allow higher energy pulses to be guided. The use of noble gases also offers the possibility to control the nonlinearity strength by changing the gas type and pressure. Furthermore, the dispersion of the waveguide provides an additional degree of freedom for tailoring the pulse propagation. Indeed, working with normal waveguide dispersion involves spectral broadening in rare gas-filled HC-PCFs and requires an additional element to compensate for the induced pulse chirp, such as fused silica^{48–50} or chirped mirrors,^{51,52} which introduce negative group delay dispersion (GDD). Interestingly, operating in the anomalous dispersion regime offers the possibility of generating Fourier-transform limited solitons directly from the fiber, making the system very compact. In this case, the pulse evolution along the HC-PCF is dominated by the interplay between the self-phase modulation-induced spectral broadening and the simultaneous temporal compression due to the anomalous waveguide dispersion.^{53–58}

In this work, we report on the exploitation of this nonlinear self-compression regime using an anomalous dispersion HC-PCF

filled with noble gases to develop a highly efficient and compact post-compression stage. We show that the combination of this stage with an all-fiber pump laser system at 1550 nm enables the generation of few-cycle energetic pulses with sub-50 fs duration at a high repetition rate and demonstrate the potential of this platform by generating high-harmonics down to the EUV range in solid samples. This article is organized as follows: First, we detail our experimental platform for few-cycle pulse generation and subsequent HHG, guided by numerical simulations. We then highlight the key parameters for optimizing the pulse characteristics, such as gas pressure, input pulse energy, and polarization tailoring. Finally, we report HHG in two separate experiments: (i) up to H7 in bulk ZnO in air and (ii) up to H29 in bulk MgO in vacuum, using an in-house built spectrometer.

II. EXPERIMENTAL SETUP AND NUMERICAL SIMULATIONS

A. Setup of the few-cycle pulse source at 1550 nm

The few-cycle pulsed source used in our experiments, comprising an ultrafast fiber laser and a post-compression stage, is depicted in Fig. 1(a). It consists of an erbium-doped fiber chirped-pulse amplifier system (Calmar, FLCPA-01C) operating at 1550 nm and generating pulses with a duration of 600 fs and an energy of 3 μJ at a repetition rate of 660 kHz. The linear polarization of the beam is then adjusted using waveplates, and the pulses are injected in the post-compression stage using injection optics (L_1) consisting of a two-lens telescope ($f_a = 50$ and $f_b = 125$ mm) to adjust the beam size to ~10 mm and a converging lens ($f_c = 75$ mm). The post-compression stage is based on a hybrid Kagome-type hollow-core photonic crystal fiber (HC-PCF,⁵⁹ GLOphotonics) with a 33 μm core mode-field diameter, featuring an anomalous dispersion at 1550 nm. The 2 m-long HC-PCF is placed inside a high-pressure gas cell capped at its both sides with quartz windows that are only 0.2 mm thick to minimize pulse distortion. The transmission efficiency through the argon-filled fiber assembly is higher than 80%. The out-coupled self-compressed pulses are then collimated with a lens L_2 ($f_2 = 125$ mm) and sent through a half-wave plate and a

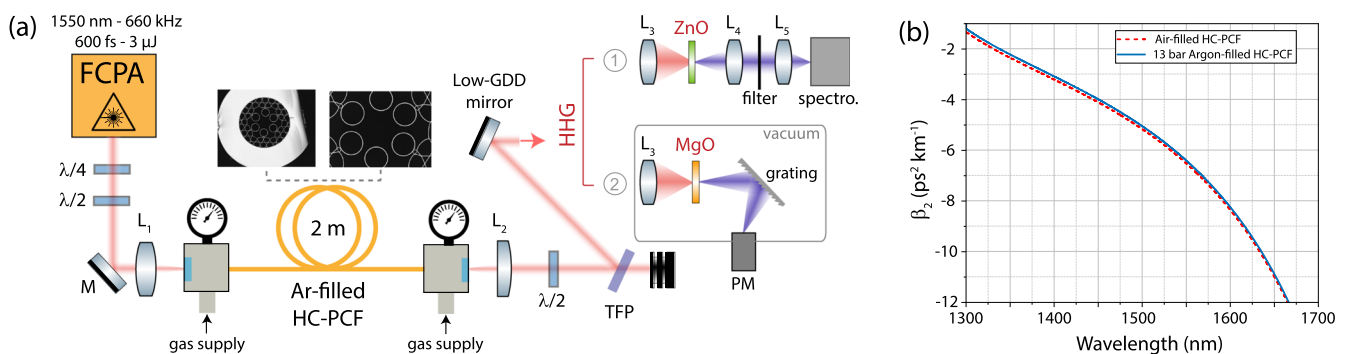


FIG. 1. (a) Experimental setup for pulse self-compression in an argon-filled hollow-core photonic crystal fiber (HC-PCF) and high-harmonic generation (HHG) in ZnO (in air) or MgO (in vacuum) samples. FCPA: fiber chirped-pulse amplifier, M: mirror, TFP: thin film polarizer, and PM: photomultiplier. *Inset:* structure of the HC-PCF. (b) Dispersion of the HC-PCF filled with argon gas at a pressure of 13 bars, obtained by combining the measured waveguide dispersion and the calculated dispersion of the argon gas.⁴⁶

thin film polarizer (TFP), which together act as a polarization filter. A low GDD mirror is then used to direct the beam toward the HHG section. Temporal and spectral characterization of the output laser waveforms was performed at this stage using an autocorrelator (APE pulseCheck, 1.5 ps time scan), an optical spectrum analyzer (Anritsu MS9740A, 0.6–1.75 μm), and a second harmonic generation frequency resolved optical gating (SHG-FROG) system. Subsequently, two HHG schemes were investigated and are described in detail in Secs. II B–III C: (i) using a ZnO crystal in air and (ii) using a MgO crystal in a vacuum chamber comprising a home-built EUV spectrometer.

B. Numerical modeling of pulse self-compression in a gas-filled HC-PCF

First, we numerically studied the temporal and spectral pulse evolutions during propagation along the HC-PCF using commercial software (fiberdesk⁶⁰). This software is based on the resolution of the scalar nonlinear Schrödinger equation (NLSE):

$$\frac{\partial A}{\partial z} = -\frac{\alpha}{2}A + \sum_{n \geq 2} \beta_n \frac{i^{n+1}}{n!} \frac{\partial^n A}{\partial T^n} + iy \left(1 + \frac{i}{\omega_0} \frac{\partial}{\partial t} \right) A |A|^2, \quad (1)$$

where A is the slowly varying complex pulse envelope, α represents the linear losses in the fiber, β_n is the n th order dispersion coefficient, and γ corresponds to the contribution from the Kerr nonlinearity through self-phase modulation and is defined as $\gamma = \frac{2\pi n_2}{\lambda A_{eff}}$, in which n_2 is the nonlinear index at wavelength λ (corresponding to a carrier frequency ω_0) and A_{eff} is the effective mode field area. As light is highly confined in the gas-filled core of the HC-PCF, the nonlinear refractive index is determined by the gas pressure as $n_2 = P(\text{bar}) \times 9.8 \times 10^{-24} \text{ (m}^2/\text{W)}$.⁶¹ The term with the

first temporal derivative accounts for self-steepening. The calculated dispersion curve for the fundamental mode guided in the argon-filled fiber is shown in Fig. 1(b). It results from two contributions: the waveguide group velocity dispersion (GVD) (β_2^{WG}) derived from the effective index of the fundamental mode calculated using a finite element method (FEM) considering an air-filled fiber at atmospheric pressure and the GVD of the pressurized argon (β_2^{gas}). The total dispersion is then calculated using the following approximation:

$$\beta_2(\lambda, P) \approx \frac{\lambda^3}{2\pi c^2} \left(\frac{P}{P_0} \frac{\partial^2 \chi_e}{\partial \lambda^2} + \frac{\partial^2 n_{eff}^{01}}{\partial \lambda^2} \right) = \beta_2^{gas} + \beta_2^{WG}, \quad (2)$$

where n_{eff}^{01} is the effective index of the LP₀₁ mode guided in the air-filled fiber, c is the speed of light, P is the gas pressure, P_0 is the atmospheric pressure, and $\chi_e(\lambda)$ represents the Sellmeier expansion of the electric susceptibility of the gas at room temperature.^{62,63} As shown in Fig. 1(b), for 13 bar argon pressure, our fiber exhibits a second order group velocity dispersion (GVD) $\beta_2 \approx -6.4 \text{ (ps}^2/\text{km)}$. The higher order dispersion terms calculated from the dispersion curve using a polynomial fit are as follows: $\beta_3 \approx +401 \text{ (fs}^3/\text{cm)}$ and $\beta_4 \approx -1872 \text{ (fs}^4/\text{cm)}$. The numerical results obtained considering input pulses of 600 fs duration and 2.5 μJ are shown in Fig. 2. The pulse dynamics along the fiber shows a monotonic spectral broadening combined with significant temporal shortening, leading to strong peak power scaling. The pulse self-compression process, resulting from the interplay between self-phase modulation and anomalous dispersion, accelerates strongly in the second half of the fiber, demonstrating the feasibility of generating sub-30 fs pulses from such a platform. The calculated output pulse characteristics are shown in Figs. 2(c) and 2(d). Compressed pulses of 27 fs with more than 80 MW peak power are calculated after 2 m of propagation in

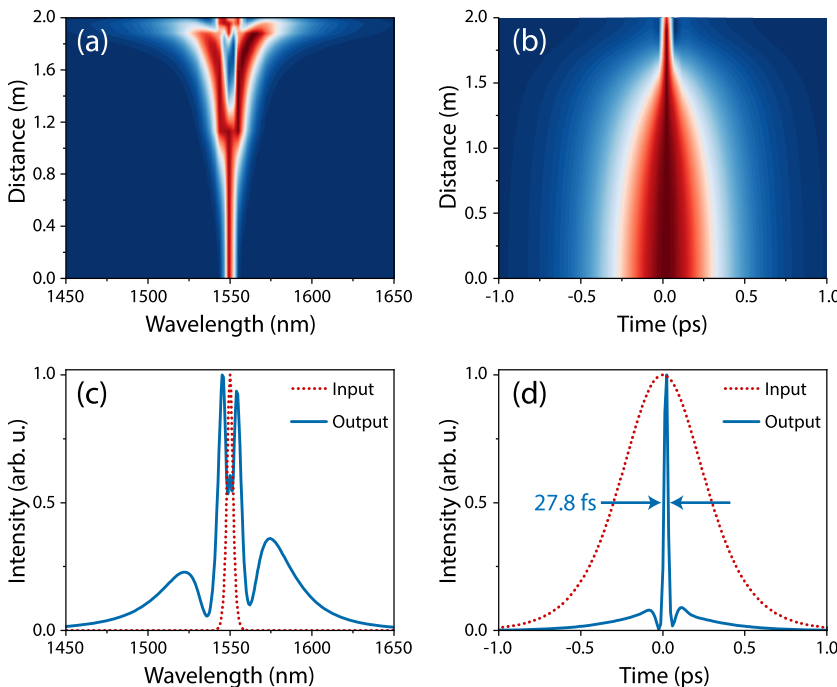


FIG. 2. Numerical simulations of pulse self-compression. (a) Spectral and (b) temporal evolutions of the pulse as a function of distance along the fiber. (c) Spectrum of the multi-cycle input pulse compared with the broad spectrum at the HC-PCF output. (d) Temporal profile of the compressed pulse and its comparison with the input pulse.

the nonlinear fiber. This corresponds to a compression factor greater than 22. It is worth noting the asymmetric distribution of the output spectrum due to third-order dispersion and self-steepening.

III. EXPERIMENTAL RESULTS

A. Few-cycle pulse optimization

First, we performed measurements without the polarization components by following the evolution of the pulse duration at the fiber output as the input pulse energy was increased at different argon pressures, as shown in Fig. 3(a). At a pressure of 11 bars, we observed that pulse compression reached its optimum at an input energy level of $2.5 \mu\text{J}$. The 600 fs input pulses are then compressed down to 50 fs. At lower pressures, the self-compression regime is not reached due to low accumulated nonlinearity. Conversely, at higher pressures, the energy required to reach the sub-50 fs regime was significantly reduced. The typical output spectra measured at 13 bars of argon pressure for different input pulse energy levels are shown in Fig. 3(b). As expected, a strong spectral broadening is observed with increasing pulse energy before reaching the self-compression regime above the $2 \mu\text{J}$ energy level. The typical autocorrelation trace measured for a gas pressure of 13 bars and $2.5 \mu\text{J}$ input energy is shown in Fig. 4(b). The pulse duration derived from the AC trace assuming a Gaussian pulse shape is ~ 60 fs, corresponding to ~ 11 optical cycles at 1550 nm. However, the AC trace exhibited a notable pedestal of more than 60% of the total pulse energy. This is very different from numerical predictions, which suggests that pulse propagation is affected by additional effects.

Note that when self-compression is reached, we observe the generation of visible light at 515 nm, corresponding to the third

harmonic of the pump signal at 1545 nm. The corresponding spatial distribution exhibits a “supermode” structure resulting from the coupling between the LP02 core mode and the cladding mode, as shown in Fig. 4(a). The output power at 515 nm evolves linearly with the pump power, with a threshold level of about $1.65 \mu\text{J}$. The maximum power measured at 515 nm is ~ 1 mW.

To enhance the contrast of the compressed pulses, we have incorporated a set of half-wave and quarter-wave plates before and after the hollow core fiber in combination with a thin-film polarizer (TFP) placed at the post-compressor output. This polarization filter is combined with a long pass spectral filter to simultaneously select the fundamental mode of the fiber core and suppress the visible light. This has resulted in significant pulse contrast enhancement, as shown in Fig. 5(a). Indeed, more than 70% of the energy is now concentrated in the main pulse peak, which is well-fitted with a Gaussian pulse with a duration of 48 fs. The output beam exhibits a Gaussian spatial distribution, indicating an efficient fundamental mode filtering. This observation confirms that polarization filtering is an efficient approach to improve pulse purity by suppressing the cladding modes, which interact less with the gas and thus contribute more to the pedestal. It should be noted that the filtered pulses are narrower than those measured directly at the fiber output due to the limited transmission bandwidth of the TFP used in the experiments. Despite this filtering effect, the pulses exiting the post-compressor at $2.5 \mu\text{J}$ can reach their Fourier transform limit with sub-50 fs duration, as shown in Fig. 5(a). It is also worth noting that the beam shape of the rejected polarization containing the non-compressed pulse also exhibits a Gaussian-like shape, indicating that propagation within the fiber is dominated by the fundamental mode guidance. It is highly expected that the fiber bending-induced

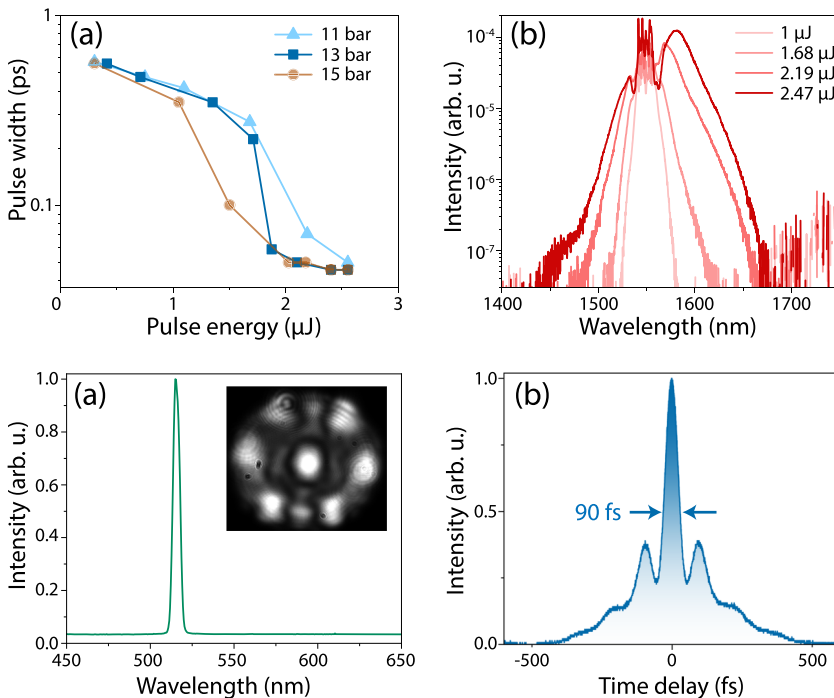


FIG. 3. (a) Measured pulse durations for different argon pressures and different input pulse energies. (b) Output spectra measured at 13 bars of gas pressure for different pulse energy levels.

FIG. 4. (a) Spectrum of the third harmonic generation (THG) generated inside the HC-PCF. Inset: spatial distribution of THG. (b) Corresponding autocorrelation trace measured at 1550 nm.

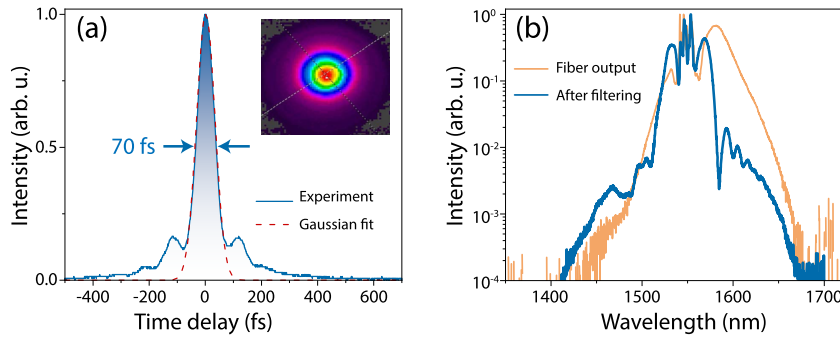


FIG. 5. Pulse features after polarization and spectral filtering. (a) Autocorrelation trace. *Inset:* near-field distribution of the output beam. (b) Optical spectrum before and after filtering.

birefringence is behind this degeneracy lifting, as evidenced in Ref. 64. This could explain the limitation in post-compression efficiency. More work would be needed to explore this avenue and provide solutions for improvements.

The output pulse energy measured after the polarization filter is about $0.92 \mu\text{J}$ for an input energy of $2.5 \mu\text{J}$, giving an overall efficiency of 37%. To explore the potential of this source to produce shorter pulses as predicted numerically, we have replaced the TFP with a polarization beam splitter (PBS) and performed second harmonic generation frequency-resolved optical-gating (SHG-FROG) pulse characterization. The results obtained for a gas pressure of 13 bars and an input energy of $2.5 \mu\text{J}$ are shown in Fig. 6. These measurements confirm that our platform is very attractive for the generation of few-cycle pulses with sub-40 fs. Indeed, the recovered spectrum exhibits a strongly structured spectral shape with good qualitative agreement with experiments. The pulse duration derived from phase retrieval calculations is very close to the Fourier-transform limited duration inferred from the measured spectrum

assuming a zero-phase relationship. The main limitation of these measurements comes from the low spectral resolution of our FROG instrument, which is $\sim 9 \text{ nm}$. Work is under way to fix this issue. The power efficiency of this configuration was lower than that of the TFP-based scheme, with a maximum extracted energy of $\sim 0.6 \mu\text{J}$.

B. High-harmonic generation in ZnO

The compressed pulses obtained using the TFP-based scheme (50 fs pulses with $0.92 \mu\text{J}$ of energy) were then focused into a $500 \mu\text{m}$ thick ZnO sample to obtain HHG. Using a focal length of 35 mm, the beam spot size was $\sim 20 \mu\text{m}$, which corresponds to an intensity of $5.8 \text{ TW}/\text{cm}^2$.

The HHG signal is observed and optimized by moving the sample around the focal point using a translation stage. The harmonics for linear polarization were measured using two fused silica lenses, with $f = 25 \text{ mm}$ to collimate the beam and $f = 50 \text{ mm}$ to inject the beam into the spectrometer (OceanOptics Maya 2000 Pro,

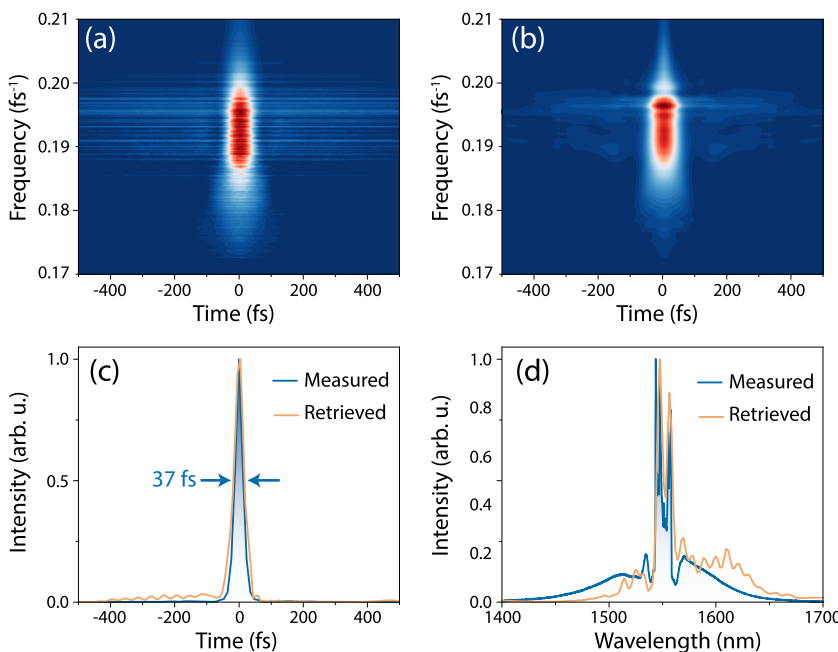


FIG. 6. SHG-FROG measurement of the post-compressed pulses using a PBS-based polarization filter. (a) Measured and (b) retrieved FROG traces. (c) Comparison between measured and retrieved pulse durations. (d) Comparison between measured and retrieved spectra.

covering a spectral range of 200–1200 nm). Spectral analysis of the transmitted beam reveals the generation of all odd harmonics up to H7, as shown in Fig. 7. We observe an additional signal that can be identified as incoherent luminescence centered at 385 nm, corresponding to the band edge emission. However, in this experiment, we were limited to measuring H7 due to our detection system.

We investigate the yields of harmonics H3, H5, H7, and the luminescence as a function of the driving laser intensity. The power was varied using an attenuator, and the intensity was estimated from the measured pulse energy and the focal spot size for a pulse duration of 50 fs. The harmonic intensities were estimated by integrating the corresponding spectra.

The H3 harmonic centered at 516 nm is selected using a Semrock F01-940/SP-25-D transmission filter. The harmonic intensity grows with increasing pump power and begins to saturate at higher pump levels. It can be well fitted with the polynomial expression $[I^{(n)} = I(t)^q]$,^{22,37} where $I^{(n)}$ is the intensity of the nth harmonic and $I(t)$ is the intensity of the driving laser. We obtain $q = 3.2$, which implies that H3 is dominated by the perturbative contribution, as shown in Fig. 7(b). The H5 harmonic is selected using a highly reflective laser mirror at 308 nm. The corresponding efficiency slope follows a perturbative scaling law at a low laser intensity ($q = 5$) and deviates from this behavior at high intensities with non-perturbative scaling ($q = 1.7$) [Fig. 7(c)]. H7 is selected using a Pelham 220-BB-1D VUV/UV transmission filter, which is adapted for the measurement of spectra around 220 nm with a typical bandwidth of 35–50 nm (FWHM), although H3 (516.6 nm) and H5 (310 nm) are partially transmitted due to their high energies while the residual IR pump is highly attenuated. H7 is well above the gap and scales non-perturbatively [$q = 4.7$, Fig. 7(d)]. The intensity dependent fluorescence measurement, obtained using the HRs 275–350 nm Topas filter that can reflect both H5 and luminescence, is shown in [Fig. 7(e)]. For a pure ZnO crystal, without defects and/or doping, at least four photons at $1.55 \mu\text{m}$ are necessary to overcome the bandgap. At low laser intensities, the multiphoton absorption dominates, confirmed by a value $q = 3.8$ of the fluorescent signal.

C. High harmonic generation in MgO

To explore the capabilities of our laser system to drive EUV harmonics, we build a second HHG bench using a $200 \mu\text{m}$ thick MgO bulk sample, which is integrated into a vacuum chamber that also contains the focusing lens and the EUV spectrometer, as shown in Fig. 1(b). The laser beam is focused on the MgO crystal at normal incidence, and the EUV signal is optimized by moving the sample on a motorized translation stage along the optical axis. The interaction of the intense laser pulse with the MgO sample (bandgap $\Delta E = 7.8 \text{ eV}$) results in the emission of coherent high-order harmonics in the EUV range, which co-propagate with the driving laser. The fundamental beam and high order harmonics are spectrally resolved using a home-built EUV spectrometer consisting of a reflective concave diffraction grating (McPherson 234/302, 2400 grooves/mm, Pt-coated) and a photomultiplier. Spectra were acquired by scanning and counting photons at each wavelength step for 10 s. The crystal was continuously moved during the scan with a speed of $20 \mu\text{m}$ per second to avoid any heating-induced damage. The range of harmonics detected is shown in the spectrum in Fig. 8(a), recorded at a pump intensity of 5.4 TW cm^{-2} . As can be seen, non-perturbative harmonics are generated up to H29, well above the material bandgap, demonstrating the relevance of our fiber-based laser platform for HHG. We have also studied the scaling of individual harmonic peaks by varying the pump laser intensity from 3 to 5.8 TW cm^{-2} . The results corresponding to harmonics H19, H21, and H23 are shown in Fig. 8(b). For comparison, we show the theoretical scaling curve for a 19th-order process. At lower intensities, the harmonics are highly nonlinear with a very close generation efficiency but still below the perturbative regime, while at higher intensities, the scaling efficiency is reduced indicating the non-perturbative nature of the high-order harmonics. The photon flux of all combined harmonics is measured to be more than 10^6 photons/s, taking into account the grating efficiency and the quantum efficiency of the photomultiplier. This corresponds to an HHG energy of a few pW for a pump energy of 450 mW ($0.68 \mu\text{J}$ @ 660 kHz) and, therefore, to an efficiency of 10^{-11} .

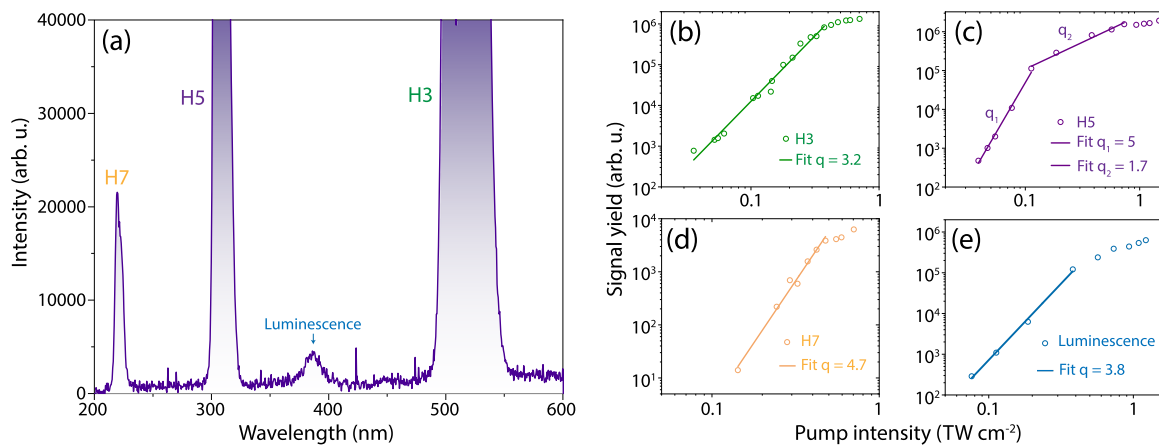


FIG. 7. (a) Typical HHG spectrum in a ZnO sample, measured at a pump intensity of 1 TW cm^{-2} . (b)–(d) Intensity-dependence of the high-order harmonic yields for (b) below-gap (H3), (c) near-gap (H5), and (d) far above-gap (H7) harmonics. (e) Intensity dependence of the luminescence.

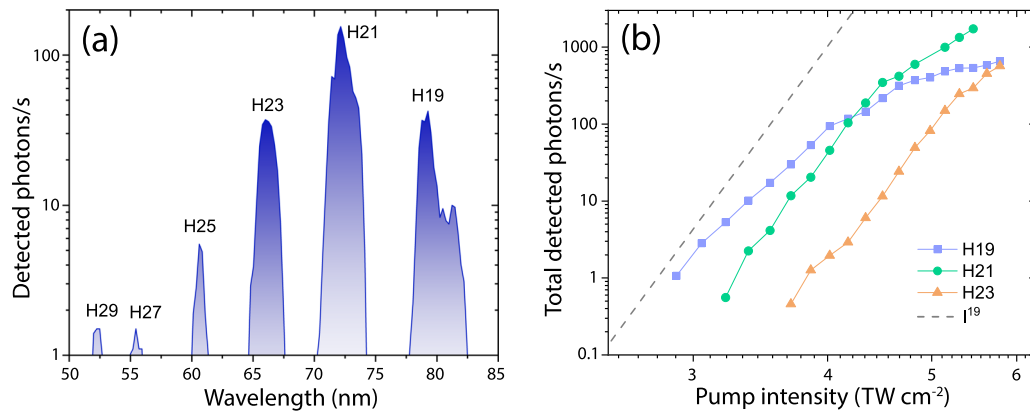


FIG. 8. EUV HHG in a 200 μm thick MgO crystal. (a) HHG spectrum generated for a pump laser intensity of 5.4 TW cm^{-2} . (b) Signal yields as a function of pump intensity and comparison with a 19th-order scaling.

Even though such a bulk-HHG cannot compete with gas-HHG in terms of yield and photon energy for now, it offers the possibility to realize compact, solid-state attosecond sources in spectral ranges inaccessible to the generation in gases, such as the terahertz gap and the EUV. In addition, such sources can be pumped using high-repetition-rate lasers, which could prove relevant for imaging applications.

IV. CONCLUSION

In conclusion, we have demonstrated the realization of a high energy, few-cycle fiber laser qualified for high harmonic generation in solids. The compact laser platform combines an erbium-doped fiber chirped pulse amplifier with a post-compression stage featuring an Ar-filled hollow-core photonic crystal fiber. The interplay between anomalous dispersion and the Kerr nonlinearity enables the generation of fundamental solitons with more than 18 MW peak power and sub-50 fs duration. This few-cycle laser source holds great promise for a wide range of strong field-driven experiments in dense media, such as HHG and terahertz generation. Indeed, our results show that perturbative and non-perturbative harmonics up to H7 could be efficiently generated in bulk ZnO samples. Using a MgO crystal, we also demonstrated the generation of EUV harmonics in the vicinity of 70 nm wavelength. There is still room for optimizing the source by increasing the efficiency of the post-compression stage. This could be achieved by optimizing the fiber design to reduce the impact of higher-order modes. The use of broadband polarization beam splitters is very promising for the generation of sub-30 fs pulses. In terms of HHG optimization, the exploration of large bandgap materials with higher damage thresholds is one of the routes to energy scaling in the EUV.

ACKNOWLEDGMENTS

The authors acknowledge the financial support from the French Agence Nationale de la Recherche through the Flex-UV (Grant

No. ANR-20-CE42-0013) and ATTOCOM (Grant No. ANR-21-CE30-0036) projects and from the European Commission through the OPTOLOGIC (H2020-FET OPEN, Grant No. 899794) and MIMOSA (European Innovation Council, Grant No. 101046651) projects.

AUTHOR DECLARATIONS

Conflict of Interest

The authors have no conflicts to disclose.

Author Contributions

D. Boukhaoui: Formal analysis (equal); Investigation (lead); Writing – original draft (supporting). **A. Mikhneva:** Formal analysis (equal); Visualization (equal). **S. Idlahcen:** Data curation (equal); Investigation (equal). **J. Houard:** Formal analysis (equal); Investigation (equal); Methodology (equal). **T. Godin:** Data curation (equal); Funding acquisition (supporting); Investigation (supporting); Writing – original draft (equal); Writing – review & editing (equal). **L. Guiramand:** Investigation (equal). **I. Blum:** Formal analysis (supporting); Investigation (supporting). **F. Amrani:** Formal analysis (supporting); Investigation (supporting). **F. G er me:** Investigation (supporting); Writing – original draft (supporting). **F. Benabid:** Investigation (supporting). **D. Gauthier:** Investigation (supporting); Writing – original draft (supporting). **W. Boutu:** Investigation (supporting); Writing – original draft (supporting). **H. Merdji:** Investigation (supporting). **A. Vella:** Data curation (equal); Funding acquisition (lead); Writing – original draft (supporting). **A. Hideur:** Data curation (equal); Funding acquisition (lead); Methodology (lead); Supervision (lead); Writing – original draft (equal).

DATA AVAILABILITY

The data that support the findings of this study are available from the corresponding author upon reasonable request.

REFERENCES

- ¹M. Ferray, A. L'Huillier, X. Li, L. Lompre, G. Mainfray, and C. Manus, "Multiple-harmonic conversion of 1064 nm radiation in rare gases," *J. Phys. B: At., Mol. Opt. Phys.* **21**, L31 (1988).
- ²A. L. Cavalieri, N. Müller, T. Uphues, V. S. Yakovlev, A. Baltuška, B. Horvath, B. Schmidt, L. Blümel, R. Holzwarth, S. Hendel *et al.*, "Attosecond spectroscopy in condensed matter," *Nature* **449**, 1029–1032 (2007).
- ³P. Wernet, J. Gaudin, K. Godehusen, O. Schwarzkopf, and W. Eberhardt, "Femtosecond time-resolved photoelectron spectroscopy with a vacuum-ultraviolet photon source based on laser high-order harmonic generation," *Rev. Sci. Instrum.* **82**, 063114 (2011).
- ⁴T. Popmintchev, M.-C. Chen, P. Arpin, M. M. Murnane, and H. C. Kapteyn, "The attosecond nonlinear optics of bright coherent X generation," *Nat. Photonics* **4**, 822–832 (2010).
- ⁵P. Agostini and L. F. DiMauro, "The physics of attosecond light pulses," *Rep. Prog. Phys.* **67**, 1563 (2004).
- ⁶M. Hentschel, R. Kienberger, C. Spielmann, G. A. Reider, N. Milosevic, T. Brabec, P. Corkum, U. Heinzmann, M. Drescher, and F. Krausz, "Attosecond metrology," *Nature* **414**, 509–513 (2001).
- ⁷G. Sansone, E. Benedetti, F. Calegari, C. Vozzi, L. Avaldi, R. Flammini, L. Poletto, P. Villoresi, C. Altucci, R. Velotta *et al.*, "Isolated single-cycle attosecond pulses," *Science* **314**, 443–446 (2006).
- ⁸E. Goulielmakis, M. Schultze, M. Hofstetter, V. S. Yakovlev, J. Gagnon, M. Uiberacker, A. L. Aquila, E. Gullikson, D. T. Attwood, R. Kienberger *et al.*, "Single-cycle nonlinear optics," *Science* **320**, 1614–1617 (2008).
- ⁹K. Zhao, Q. Zhang, M. Chini, Y. Wu, X. Wang, and Z. Chang, "Tailoring a 67 attosecond pulse through advantageous phase-mismatch," *Opt. Lett.* **37**, 3891–3893 (2012).
- ¹⁰J. Itatani, J. Levesque, D. Zeidler, H. Niikura, H. Pépin, J.-C. Kieffer, P. B. Corkum, and D. M. Villeneuve, "Tomographic imaging of molecular orbitals," *Nature* **432**, 867–871 (2004).
- ¹¹W. Li, X. Zhou, R. Lock, S. Patchkovskii, A. Stolow, H. C. Kapteyn, and M. M. Murnane, "Time-resolved dynamics in N₂O₄ probed using high harmonic generation," *Science* **322**, 1207–1211 (2008).
- ¹²P. Peng, C. Marceau, and D. M. Villeneuve, "Attosecond imaging of molecules using high harmonic spectroscopy," *Nat. Rev. Mater.* **1**, 144–155 (2019).
- ¹³C. Vozzi, M. Negro, F. Calegari, G. Sansone, M. Nisoli, S. De Silvestri, and S. Stagira, "Generalized molecular orbital tomography," *Nat. Phys.* **7**, 822–826 (2011).
- ¹⁴M. Negro, M. Devetta, D. Faccialá, S. De Silvestri, C. Vozzi, and S. Stagira, "High-order harmonic spectroscopy for molecular imaging of polyatomic molecules," *Faraday Discuss.* **171**, 133–143 (2014).
- ¹⁵S. Haessler, J. Caillat, W. Bouto, C. Giovanetti-Teixeira, T. Ruchon, T. Auguste, Z. Diveki, P. Breger, A. Maquet, B. Carré *et al.*, "Attosecond imaging of molecular electronic wavepackets," *Nat. Phys.* **6**, 200–206 (2010).
- ¹⁶C. Vozzi, R. Torres, M. Negro, L. Brugnera, T. Siegel, C. Altucci, R. Velotta, F. Frassetto, L. Poletto, P. Villoresi *et al.*, "High harmonic generation spectroscopy of hydrocarbons," *Appl. Phys. Lett.* **97**, 241103 (2010).
- ¹⁷G. Sansone, "Looking into strong-field dynamics," *Nat. Photonics* **14**, 131–133 (2020).
- ¹⁸C. Chappuis, D. Bresteau, T. Auguste, O. Gobert, and T. Ruchon, "High-order harmonic generation in an active grating," *Phys. Rev. A* **99**, 033806 (2019).
- ¹⁹A. Palacios and F. Martín, "The quantum chemistry of attosecond molecular science," *Wiley Interdiscip. Rev.:Comput. Mol. Sci.* **10**, e1430 (2020).
- ²⁰P. M. Kraus, M. Zürich, S. K. Cushing, D. M. Neumark, and S. R. Leone, "The ultrafast X-ray spectroscopic revolution in chemical dynamics," *Nat. Rev. Chem.* **2**, 82–94 (2018).
- ²¹J. Marangos, "Development of high harmonic generation spectroscopy of organic molecules and biomolecules," *J. Phys. B: At., Mol. Opt. Phys.* **49**, 132001 (2016).
- ²²S. Ghimire, A. D. DiChiara, E. Sistrunk, P. Agostini, L. F. DiMauro, and D. A. Reis, "Observation of high-order harmonic generation in a bulk crystal," *Nat. Phys.* **7**, 138–141 (2011).
- ²³T. T. Luu, M. Garg, S. Y. Kruchinin, A. Moulet, M. T. Hassan, and E. Goulielmakis, "Extreme ultraviolet high-harmonic spectroscopy of solids," *Nature* **521**, 498–502 (2015).
- ²⁴G. Vampa, T. Hammond, N. Thiré, B. Schmidt, F. Légaré, C. McDonald, T. Brabec, D. Klug, and P. Corkum, "All-optical reconstruction of crystal band structure," *Phys. Rev. Lett.* **115**, 193603 (2015).
- ²⁵Y. S. You, D. A. Reis, and S. Ghimire, "Anisotropic high-harmonic generation in bulk crystals," *Nat. Phys.* **13**, 345–349 (2017).
- ²⁶N. Tancogne-Dejean, O. D. Mücke, F. X. Kärtner, and A. Rubio, "Impact of the electronic band structure in high-harmonic generation spectra of solids," *Phys. Rev. Lett.* **118**, 087403 (2017).
- ²⁷M. Garg, M. Zhan, T. T. Luu, H. Lakhota, T. Klostermann, A. Guggenmos, and E. Goulielmakis, "Multi-petahertz electronic metrology," *Nature* **538**, 359–363 (2016).
- ²⁸N. Yoshikawa, T. Tamaya, and K. Tanaka, "High-harmonic generation in graphene enhanced by elliptically polarized light excitation," *Science* **356**, 736–738 (2017).
- ²⁹M. Hohenleutner, F. Langer, O. Schubert, M. Knorr, U. Huttner, S. W. Koch, M. Kira, and R. Huber, "Real-time observation of interfering crystal electrons in high-harmonic generation," *Nature* **523**, 572–575 (2015).
- ³⁰G. Ndabashimiye, S. Ghimire, M. Wu, D. A. Browne, K. J. Schafer, M. B. Gaarde, and D. A. Reis, "Solid-state harmonics beyond the atomic limit," *Nature* **534**, 520–523 (2016).
- ³¹P. G. Hawkins, M. Y. Ivanov, and V. S. Yakovlev, "Effect of multiple conduction bands on high-harmonic emission from dielectrics," *Phys. Rev. A* **91**, 013405 (2015).
- ³²X. Liu, X. Zhu, X. Zhang, D. Wang, P. Lan, and P. Lu, "Wavelength scaling of the cutoff energy in the solid high harmonic generation," *Opt. Express* **25**, 29216–29224 (2017).
- ³³Z. Guan, X.-X. Zhou, and X.-B. Bian, "High-order-harmonic generation from periodic potentials driven by few-cycle laser pulses," *Phys. Rev. A* **93**, 033852 (2016).
- ³⁴T. Kroh, C. Jin, P. Krogen, P. D. Keathley, A.-L. Calendron, J. P. Siqueira, H. Liang, E. L. Falcão-Filho, C. Lin, F. X. Kärtner, and K. H. Hong, "Enhanced high-harmonic generation up to the soft X-ray region driven by mid-infrared pulses mixed with their third harmonic," *Opt. Express* **26**, 16955–16969 (2018).
- ³⁵R. Hollinger, D. Hoff, P. Wustelt, S. Skruszewicz, Y. Zhang, H. Kang, D. Würzler, T. Jungnickel, M. Dumergue, A. Nayak *et al.*, "Carrier-envelope-phase measurement of few-cycle mid-infrared laser pulses using high harmonic generation in ZnO," *Opt. Express* **28**, 7314–7322 (2020).
- ³⁶V. Nefedova, S. Fröhlich, F. Navarrete, N. Tancogne-Dejean, D. Franz, A. Hamdoui, S. Kaassamani, D. Gauthier, R. Nicolas, G. Jargot *et al.*, "Enhanced extreme ultraviolet high-harmonic generation from chromium-doped magnesium oxide," *Appl. Phys. Lett.* **118**, 201103 (2021).
- ³⁷S. Gholam-Mirzaei, J. Beetar, and M. Chini, "High harmonic generation in ZnO with a high-power mid-IR OPA," *Appl. Phys. Lett.* **110**, 061101 (2017).
- ³⁸A. Lanin, E. Stepanov, A. Fedotov, and A. Zheltikov, "Mapping the electron band structure by intraband high-harmonic generation in solids," *Optica* **4**, 516–519 (2017).
- ³⁹R. Hollinger, P. Herrmann, V. Korolev, M. Zapf, V. Shumakova, R. Röder, I. Uschmann *et al.*, "Polarization dependent excitation and high harmonic generation from intense mid-IR laser pulses in ZnO," *Nanomaterials* **11**, 4 (2020).
- ⁴⁰S. Gholam-Mirzaei, J. E. Beetar, A. Chacón, and M. Chini, "High-harmonic generation in ZnO driven by self-compressed mid-infrared pulses," *J. Opt. Soc. Am. B* **35**, A27–A31 (2018).
- ⁴¹L. He, W. Wang, K. Tian, M. Xiang, Z. Wan, B. Hu, Y. Li, H. Wu, Z.-Y. Chen, F. Yang, and H. Liang, "Dual-wavelength spectrum-shaped mid-infrared pulses and steering high-harmonic generation in solids," *Ultrafast Sci.* **3**, 0022 (2023).
- ⁴²K. Werner, M. G. Hastings, A. Schweinsberg, B. L. Wilmer, D. Austin, C. M. Wolfe, M. Kolesik, T. R. Ensley, L. Vanderhoef, A. Valenzuela, and E. Chowdhury, "Ultrafast mid-infrared high harmonic and supercontinuum generation with n_2 characterization in zinc selenide," *Opt. Express* **27**, 2867–2885 (2019).
- ⁴³D. Franz, S. Kaassamani, D. Gauthier, R. Nicolas, M. Kholodtsova, L. Douillard, J.-T. Gomes, L. Lavoute, D. Gaponov, N. Ducros *et al.*, "All semiconductor

- enhanced high-harmonic generation from a single nanostructured cone,” *Sci. Rep.* **9**, 5663 (2019).
- ⁴⁴Y. Leventoux, M. Jedidi, L. Ferhat, C. Jimenez, I. Tiliouine, G. Granger, J.-C. Orlianges, A. Crunteanu, L. Lavoute, D. Gaponov *et al.*, “High-energy solitonic source of high harmonics,” *Proc. SPIE* **12400**, 1240017 (2023).
- ⁴⁵K. F. Lee, X. Ding, T. Hammond, M. Fermann, G. Vampa, and P. Corkum, “Harmonic generation in solids with direct fiber laser pumping,” *Opt. Lett.* **42**, 1113–1116 (2017).
- ⁴⁶E. R. Peck and D. J. Fisher, “Dispersion of argon,” *J. Opt. Soc. Am.* **54**, 1362–1364 (1964).
- ⁴⁷M. Nisoli, S. De Silvestri, and O. Svelto, “Generation of high energy 10 fs pulses by a new pulse compression technique,” *Appl. Phys. Lett.* **68**, 2793–2795 (1996).
- ⁴⁸B. E. Schmidt, P. Béjot, M. Giguère, A. D. Shiner, C. Trallero-Herrero, É. Bisson, J. Kasparian, J.-P. Wolf, D. M. Villeneuve, J.-C. Kieffer *et al.*, “Compression of 1.8 μm laser pulses to sub two optical cycles with bulk material,” *Appl. Phys. Lett.* **96**, 121109 (2010).
- ⁴⁹P. Béjot, B. Schmidt, J. Kasparian, J.-P. Wolf, and F. Legaré, “Mechanism of hollow-core-fiber infrared-supercontinuum compression with bulk material,” *Phys. Rev. A* **81**, 063828 (2010).
- ⁵⁰B. E. Schmidt, A. D. Shiner, P. Lassonde, J.-C. Kieffer, P. B. Corkum, D. M. Villeneuve, and F. Legaré, “CEP stable 1.6 cycle laser pulses at 1.8 μm ,” *Opt. Express* **19**, 6858–6864 (2011).
- ⁵¹M. Nisoli, S. De Silvestri, O. Svelto, R. Szipöcs, K. Ferencz, C. Spielmann, S. Sartania, and F. Krausz, “Compression of high-energy laser pulses below 5 fs,” *Opt. Lett.* **22**, 522–524 (1997).
- ⁵²D. Schade, F. Köttig, J. R. Koehler, M. H. Frosz, P. S. J. Russell, and F. Tani, “Scaling rules for high quality soliton self-compression in hollow-core fibers,” *Opt. Express* **29**, 19147–19158 (2021).
- ⁵³K. Mak, J. Travers, N. Y. Joly, A. Abdolvand, and P. S. J. Russell, “Two techniques for temporal pulse compression in gas-filled hollow-core kagomé photonic crystal fiber,” *Opt. Lett.* **38**, 3592–3595 (2013).
- ⁵⁴M. Gebhardt, C. Gaida, T. Heuermann, F. Stutzki, C. Jauregui, J. Antonio-Lopez, A. Schulzgen, R. Amezcua-Correa, J. Limpert, and A. Tünnermann, “Nonlinear pulse compression to 43 W GW-class few-cycle pulses at 2 μm wavelength,” *Opt. Lett.* **42**, 4179–4182 (2017).
- ⁵⁵C. Gaida, M. Gebhardt, F. Stutzki, C. Jauregui, J. Limpert, and A. Tünnermann, “Thulium-doped fiber chirped-pulse amplification system with 2 GW of peak power,” *Opt. Lett.* **41**, 4130–4133 (2016).
- ⁵⁶T. Balciunas, C. Fourcade-Dutin, G. Fan, T. Witting, A. Voronin, A. Zheltikov, F. Gerome, G. Paulus, A. Baltuska, and F. Benabid, “A strong-field driver in the single-cycle regime based on self-compression in a kagome fibre,” *Nat. Commun.* **6**, 6117 (2015).
- ⁵⁷C. Gaida, M. Gebhardt, F. Stutzki, C. Jauregui, J. Limpert, and A. Tünnermann, “Self-compression in a solid fiber to 24 MW peak power with few-cycle pulses at 2 μm wavelength,” *Opt. Lett.* **40**, 5160–5163 (2015).
- ⁵⁸D. G. Ouzounov, C. J. Hensley, A. L. Gaeta, N. Venkateraman, M. T. Gallagher, and K. W. Koch, “Soliton pulse compression in photonic band-gap fibers,” *Opt. Express* **13**, 6153–6159 (2005).
- ⁵⁹F. Amrani, J. H. Osório, F. Delahaye, F. Giovanardi, L. Vincetti, B. Debord, F. Gérôme, and F. Benabid, “Low-loss single-mode hybrid-lattice hollow-core photonic-crystal fibre,” *Light: Sci. Appl.* **10**, 7 (2021).
- ⁶⁰T. Schreiber, B. Ortaç, J. Limpert, and A. Tünnermann, “On the study of pulse evolution in ultra-short pulse mode-locked fiber lasers by numerical simulations,” *Opt. Express* **15**, 8252–8262 (2007).
- ⁶¹W. Ettoumi, Y. Petit, J. Kasparian, and J.-P. Wolf, “Generalized Miller formulae,” *Opt. Express* **18**, 6613–6620 (2010).
- ⁶²A. Börzsönyi, Z. Heiner, M. P. Kalashnikov, A. P. Kovács, and K. Osvay, “Dispersion measurement of inert gases and gas mixtures at 800 nm,” *Appl. Opt.* **47**, 4856–4863 (2008).
- ⁶³P. S. J. Russell, P. Hölzer, W. Chang, A. Abdolvand, and J. C. Travers, “Hollow-core photonic crystal fibres for gas-based nonlinear optics,” *Nat. Photonics* **8**, 278–286 (2014).
- ⁶⁴C. Röhrer, J. H. Osorio, F. Beirou, M. Maurel, B. Debord, T. Graf, F. Gérôme, F. Benabid, and M. Abdou Ahmed, “Phase shift induced degradation of polarization caused by bends in inhibited-coupling guiding hollow-core fibers,” *IEEE Photonics Technol. Lett.* **31**, 1362 (2019).